Levelized Cost of Energy-Based Economic Analysis of Microgrid Equipped with Multi Energy Storage System

Pradeep Kumar[1,*], Vipin Das[2], Asheesh K. Singh[2] and P. Karuppanan[2]

[1]*National Institute of Technology Kurukshetra, Kurukshetra, Haryana, India*
[2]*Motilal Nehru National Institute of Technology Allahabad, Prayagraj, Uttar Pradesh, India*
E-mail: pradeepkumar@ieee.org; vipindas504@gmail.com; asheesh@mnnit.ac.in; pkaru@mnnit.ac.in
[*]*Corresponding Author*

Received 17 April 2022; Accepted 27 January 2023;
Publication 16 May 2023

Abstract

Energy storage system (ESS) plays a critical role in maintaining the reliability of microgrids. ESS selection for microgrids depends on energy density, specific power, specific energy, and economics. This paper analyses the economic benefits of various combinations of short-, medium-, and long-term ESS, i.e., multi-energy storage systems (MESS) in a microgrid. The economic feasibility of the system is analyzed using Homer software. The net present cost (NPC), the Levelized cost of energy (LCOE), and pollutant gas emission are chosen as parameters for analyzing the economic feasibility of the microgrids. The results show that amongst all the scenarios, the system with Hydrogen Storage System (HSS) with Proton exchange membrane fuel cell (PEMFC) and electrolyzer is the most feasible solution with the lowest LCOE and pollutant emission.

Keywords: Microgrids, energy storage, economics, net present cost, levelized cost of energy.

Distributed Generation & Alternative Energy Journal, Vol. 38_4, 1331–1356.
doi: 10.13052/dgaej2156-3306.38411

1 Introduction

Energy storage systems (ESS) have become an integral component of renewable energy systems (RESs) [1, 2]. They offer several advantages [3] and help mitigate the RES intermittency and improve their reliability [3, 4]. To aid this, power management systems monitor the load-generation balance, route excess RES power, and support the load in case of insufficient RES-generated power [5]. ESSs are classified based on their types and use. The different types of ESSs are mechanical, electrical, electrochemical, thermal, thermochemical, and chemical ESSs [6]. Depending on the use, they are classified as short-term, mid-term, and long-term ESS [3]. The short-term ESS supplies energy for a few seconds to a few minutes, like flywheel (FW) and supercapacitors (SC). Mid-term ESS, such as batteries and hydrogen storage systems (HSS), can supply energy for many hours to several days. Like pumped hydro (PH) power plants, long-term ESS takes weeks to months to supply energy [6]. For ESSs, specific power and specific energy are the two vital metrics. Figure 1 depicts the specific power and specific energy for various ESS [7].

Refs. [8–12] explores short-term ESS applications in the microgrid, like energy management and control strategies [13]. Refs. [14, 15] discusses the use of mid-term ESS such as lead-acid (LA) batteries, Lithium-ion (Li-ion) batteries, flow batteries, and HSS. The application of a long-term ESS pumped-hydro (PH) station is described in [16]. These references examine

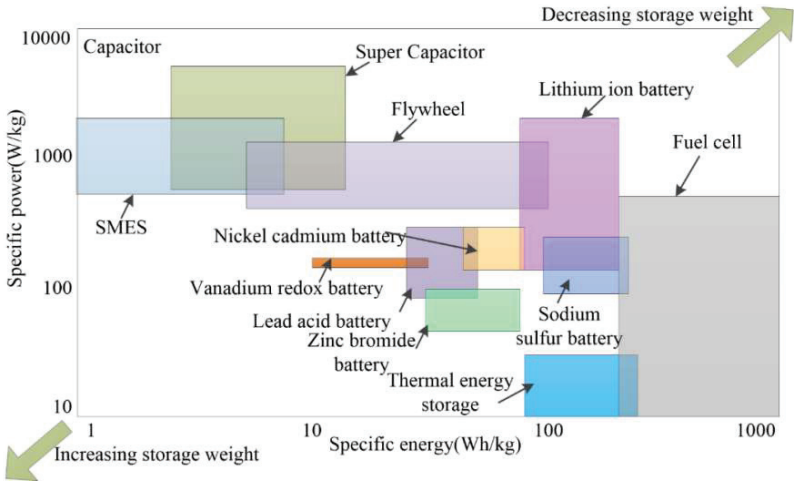

Figure 1 Specific power and a specific energy for different ESSs [4].

the technical benefits of deploying ESS in the microgrid. A few Refs. [17, 18] discuss the economic benefits of ESS using the net present cost (NPC) and Levelized cost of energy (LCOE) as critical parameters. The economic analysis of using a single ESS in microgrids is available in recent works of literature [19, 20]. However, the analysis for multiple-energy storage systems (MESS) is still unexplored.

This paper analyses the (i) economic feasibility of employing MESS and (ii) performance and technological advantage of MESS in the microgrid. The analysis is essential to find out the cost-effective combination of ESSs. The investigation is carried out using the HOMER software with the location at longitude and latitude (25°26.1′N, 81°50.8′E) in Allahabad, Uttar Pradesh, India is taken from the Homer database [21]. The economic analysis seeks to identify the ESS combination with the lowest LCOE and pollutant emission over the short-term, mid-term, and long-term. Figure 2 shows the three scenarios that are further segmented into cases. The same solar photovoltaic (PV) and load profiles are applied in each scenario. The energy density, power density, and response time of the ESS are used to analyze the performance and technological benefits. Figure 3 depicts the various ESSs employed in this work. In each example, a combination of two ESSs is employed. The results show that the MESS offers better performance than the ESSs. Also, the

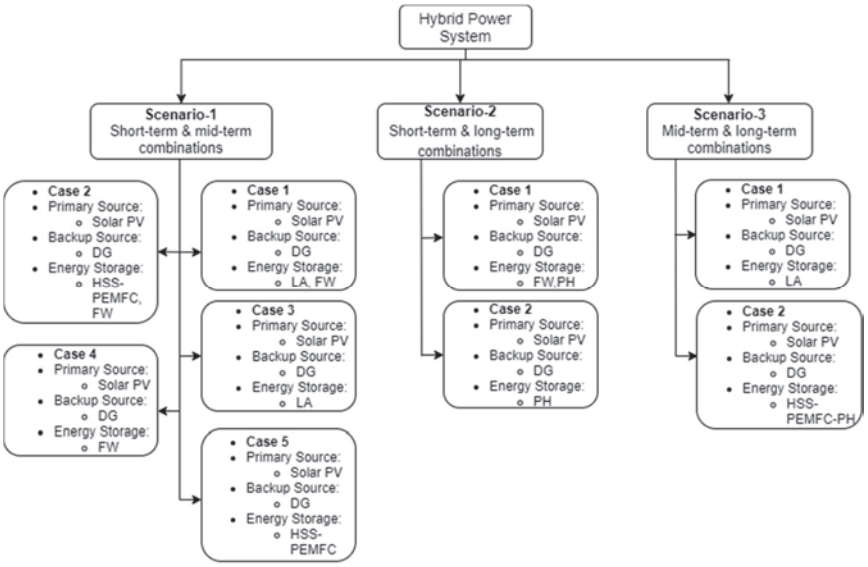

Figure 2 Different scenarios and cases used in the study.

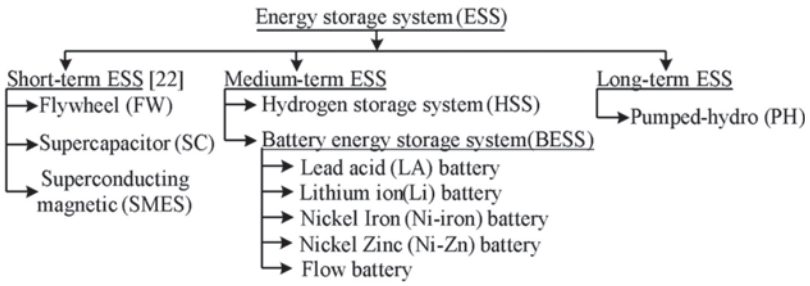

Figure 3 Various ESS technologies used in this work [3].

combination of HSS, PEMFC, electrolyzer, and PH offers the most feasible solution owing to the lowest LCOE and minimum value of emissions. Finally, a sensitivity analysis is performed to observe the impact of change in the SoC limit on the LCOE.

The rest of the paper is organized as Section 2 discusses the system architecture and the mathematical models. Problem formulation is presented in Sections 3, and results are discussed in Section 4. Finally, conclusions are drawn in Section 5.

2 System Description

2.1 System Architecture

The system is a hybrid power system (HPS) with solar-PV, diesel generator (DG), ESS, and AC loads, as shown in Figure 4. The DG is an additional energy source, which is connected to the AC bus, along with AC loads. The ESS and solar PV are connected to the DC bus. The AC and DC buses are connected through a power electronic converter specifically, a dc-dc unidirectional converter, a dc-dc bi-directional converter, and an inverter to interconnect the DC-AC system. The ESSs are a combination of different ESSs, termed MESS. They are varied as short-term, mid-term, and long-term combinations of ESS, as shown in Figure 3 for the economic analysis. The modeling of these components is discussed in the next section. Table 1 shows the ratings of the components used.

2.2 Mathematical Model

This section describes the mathematical model of the components, as depicted in Figure 5.

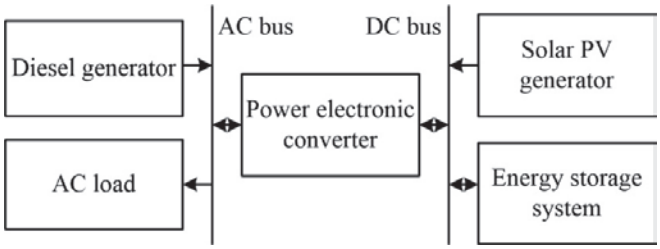

Figure 4 The structure of the HPS.

Table 1 Ratings of the components used in the HPS

Component	Solar PV	DG	LA Battery	FW	HSS	PEMFC	PH
Rating	2000 kW	1500 kW	4000kWh	1500 kW	2000 L	2000 kW	2000 kW

2.2.1 Solar-PV modeling

The simplified model (1) is used to extract power from solar PV, illustrating the output characteristics of the solar PV panel as irradiance and temperature change. The output power of a solar PV system can be expressed as [21],

$$P_{pv}(t) = D_{pv} P_{PV,rated} \frac{G(t)}{G_{STC}} (\beta_t (T(t) - T_{STC})) \tag{1}$$

2.2.2 PEMFC modeling

The power output from the PEMFC (PFC) is given as [21],

$$P_{FC}(t) = P_{in}(t)\eta_{FC} \tag{2}$$

2.2.3 Energy storage system (ESS)

This paper employs various ESS combinations to determine the optimal ESS-RES combination for lowering the LCOE and NPC. ESS components include an LA battery, FW, HSS, and PH.

2.2.3.1 *Battery and FW*

The ESS's energy generation is significantly dependent on the State of Charge (SoC). The energy produced by the ESS is denoted by [21],

$$E_{ESS}(t) = E_{ESS}(t-1) + E_{surplus}(t) \times \eta_{cc} \times \eta_{ch} \tag{3}$$

The constraint limiting the charging and discharging of the ESS can be expressed as,

$$SoC_{\min} \leq SoC(t) \leq SoC_{\max} \tag{4}$$

The minimum value of SoC is obtained in terms of the depth of discharge (DOD) as:

$$SoC_{\min} = 1 - DOD \tag{5}$$

2.2.3.2 *PH station*

The PH station stores energy as potential energy; the energy stored in a PH station can be expressed as,

$$E = 9.81\rho_w V_r h\eta \tag{6}$$

2.2.3.3 *Electrolyzer and hydrogen tank*

The electrolyzer chamber electrolyzes water using solar PV electricity. As a result, (7) gives the power transmitted from the electrolyzer for hydrogen production [21].

$$P_{ele} = P_{ren} \times \eta_{ele} \tag{7}$$

The energy output of the hydrogen storage tank is denoted as [21],

$$E_{HSS}(t) = E_{HSS}(t-1) + [P_{ele}(t) - (P_{FC}(t)/\eta_s)] \times \Delta t \tag{8}$$

2.2.4 Load modeling

For the present study, the load profile of an educational institute located in Allahabad, Uttar Pradesh, India, with location coordinates as longitude and latitude (25°26.1′N, 81°50.8′E), as shown in Figure 5. Figure 6 depicts the monthly average load profile and its variance using box plots. Since the site is an educational institution, the peak time is 10:00 AM to 5:00 PM. The bold line shows the average power, which remains nearly constant in the middle months and decreases towards the end of the year, the lowest being in July.

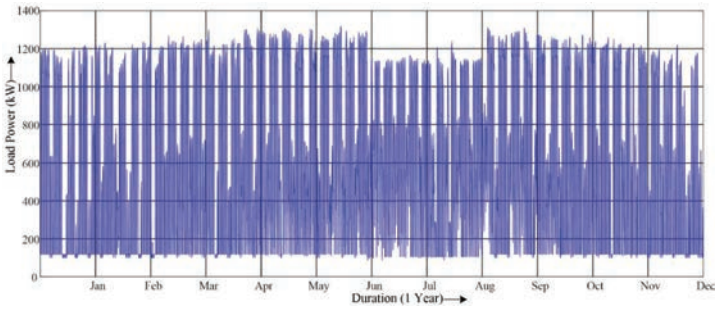

Figure 5 Yearly load profile.

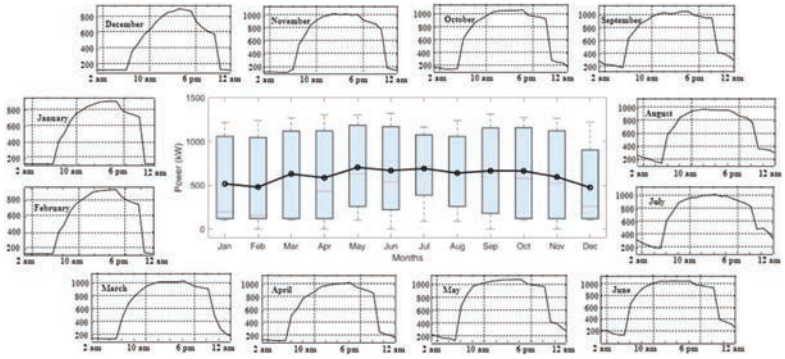

Figure 6 Monthly average load profile (hourly) with box plots.

Based on the peak and average loads of 1317.9 kW and 619.75 kW, the total energy demand is estimated to be 18874 kWh/day. The load factor is 0.47.

2.2.5 Power electronics converter

A bidirectional DC-DC converter provides power flow between the DC and the AC bus. The converter rating is determined by the maximum power rating of the ESS. The converter's primary role is to maintain the load-generation balance with the assistance of an energy management system.

3 Problem Formulation

The economic analysis of the proposed HPS is conducted using Homer pro software [21]. For the economic analysis, NPC and LCOE have been considered. These factors determine the most cost-effective solution. NPC represents the present value of the installation and system operation costs over its lifespan. It is determined as per the total annualized cost ($/year) and capital recovery factor (CRF) [22]. LCOE is the system's 'average cost per kWh' of useful electricity produced. The optimization problem is formulated to reduce the cost and carbon emission of the HPS.

3.1 Objective function

The minimization of NPC and emission are the objective function of this work. The NPC of the HPS can be given as [21]:

$$NPC = \frac{C_{at}}{\mathrm{CRF}} \tag{9}$$

The CRF and C_{at} be expressed as,

$$CRF = \frac{i(1+i)^{N_{proj}}}{(1+i)^{N_{proj}} - 1} \tag{10}$$

$$C_{at} = \xi_{a,C} + \xi_{a,O\&M} + \xi_{a,R} \tag{11}$$

The different cost components in (12) can are given as

$$\xi_{a,C} = \xi_C \times CRF \tag{12}$$

$$\xi_{a,O\&M} = \xi_{O\&M} \times t_{O\&M} \tag{13}$$

$$\xi_{a,R} = \xi_R \times F_R \times S_{FF}(i, N_{com}) - S \times S_{FF}(i, N_{com}) \tag{14}$$

The factor F_R in (15) accounts for the difference between the component and the project lifetime.

$$F_R = \begin{cases} \dfrac{CRF(i, N_{proj})}{CRF(i, N_R)}; & N_{proj} > 0 \\ 0; & N_{proj} = 0 \end{cases} \tag{15}$$

The N_R can be expressed as [21]:

$$N_R = N_{com} \times INT\left(\frac{N_{proj}}{N_{com}}\right) \tag{16}$$

Where INT stands for the integer value.
The salvage value of the component can be expressed as:

$$S = \xi_R \times \frac{N_{rem}}{N_{com}} \tag{17}$$

$$N_{rem} = N_{com} - (N_{proj} - N_R) \tag{18}$$

The S_{FF} in (14) to calculate the future value of the annual cash flow as:

$$S_{FF} = \frac{i}{(1+i)^N - 1} \tag{19}$$

For calculating the economic viability of the system, the LCOE is calculated as follows

$$LCOE = \frac{C_{at}}{E_{a,d}} \tag{20}$$

Thus, the objective function for minimization of NPC and emission ψ can be given as:

$$F = Min(C_{at}) \tag{21}$$

$$\psi = Min(\psi_{CO_2} + \psi_{CO} + \psi_{UHC} + \psi_{PM} + \psi_{SO_2} + \psi_{NO_x}) \tag{22}$$

3.2 Constraints

The objective function is optimized considering the constraints listed below.

3.2.1 Power reliability constraint

The annual unmet load (L_{unmet}), a ratio of total capacity shortage ($L_{shortage}$) to the E_a, d is considered as the power reliability constraint, given as

$$L_{unmet} = \frac{L_{shortage}}{E_{a,d}} \tag{23}$$

3.2.2 ESS constraints

The ESS constraints is the maximum ($E_{ESS,max}$) and minimum ($E_{ESS,min}$) capacity limit of the ESS, given as,

$$E_{ESS,\min} \leq E_{ESS}(t) \leq E_{ESS,\max} \tag{24}$$

$E_{ESS,max}$, and $E_{ESS,min}$ are a function of the battery SoC:

$$E_{ESS,\max} = \frac{N_{ESS} V_{ESS} B_{ah}}{1000} \times SoC_{\max} \tag{25}$$

$$E_{ESS,\min} = \frac{N_{ESS} V_{ESS} B_{ah}}{1000} \times SoC_{\min} \tag{26}$$

3.2.3 Upper and lower bounds

It consists of the maximum, and minimum number of solar PV and the PEMFC expressed as,

$$0 \leq N_{PV} \leq N_{PV}^{\max} \tag{27}$$

$$0 \leq N_{FC} \leq N_{FC}^{\max} \tag{28}$$

The components and costs used in the simulation are tabulated in Tables 1 and 2.

Table 2 Cost of the components used for simulation [21]

Cost (USD)	Capital Cost (Per kW)	Replacement Cost (Per kW)	Maintenance Cost (Per Hour)
Solar PV	1800	1800	10
Diesel generator (DG)	1521	1521	0.5
LA battery	260	260	10
FW	2400	2400	7
HSS	**1400**	**1400**	**20**
PEMFC	**1500**	**1500**	**5**
Electrolyzer	**1500**	**1500**	**5**
PH station	**2638**	**2638**	**16**
Power electronics converters	400	400	20

The steps involved in the entire process are

Step 1: Calculate the load demand and available generation.
Step 2: Calculate the load-generation mismatch.
Step 3: Feed the load with Solar PV.
Step 4: If there are any unmet loads, feed the load with available ESS. The ESS with high energy density is given a priority over other ESSs.
Step 5: If ESSs are not available, then feed the load with DG.
Step 6: If there is any excess power, store the power to available ESS (Priority for high energy density ESS).
Step 7: Check whether the load-generation balance is satisfied or not; if yes, stop the simulation; else, go to step-2.

4 Results and Discussion

This paper uses the Homer to simulate the system shown in Figure 5 using equipment with ratings shown in Table 1. The analysis considers three different scenarios, each with different combinations of ESS, namely,

1. Scenario-1: short-term & mid-term ESS combinations.
2. Scenario-2: short-term & long-term ESS combinations.
3. Scenario-3: mid-term & long-term ESS combinations.

The different ESS combinations with RES and DG under each scenario are presented in Figure 2. The most cost-effective combination is chosen as the best solution for microgrid applications. The solar irradiance data for location is taken from the Homer database [21]. Figures 7(a) and 7(b) show the location's daily and monthly solar irradiance. The annual average

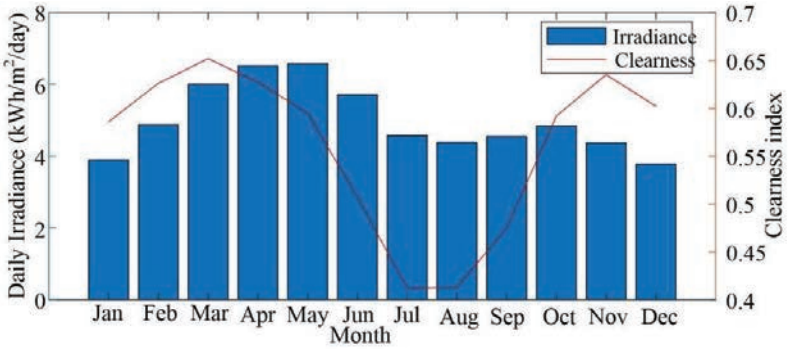

(a)

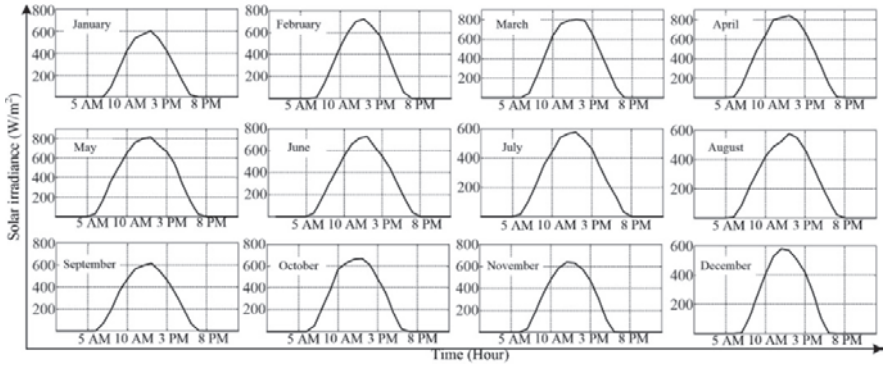

(b)

Figure 7 Solar irradiation data of the location (a) Monthly and (b) Monthly average.

solar irradiation is 4.93 kW/m^2. The simulation is conducted using Homer MATLAB® Link-based dispatch strategy.

4.1 Scenario-1

In this scenario, short-term ESS, FW is combined with mid-term ESSs, LA battery, and HSS. Based on these combinations, four cases are considered as,

(a) Case-1: Solar PV-DG-LA Battery-FW HPS.
(b) Case-2: Solar PV-DG-HSS-PEMFC-FW HPS.
(c) Case-3: Solar PV-DG-LA Battery HPS.
(d) Case-4: Solar PV-DG-FW HPS.
(e) Case-5: Solar PV-DG-HSS-PEMFC HPS.

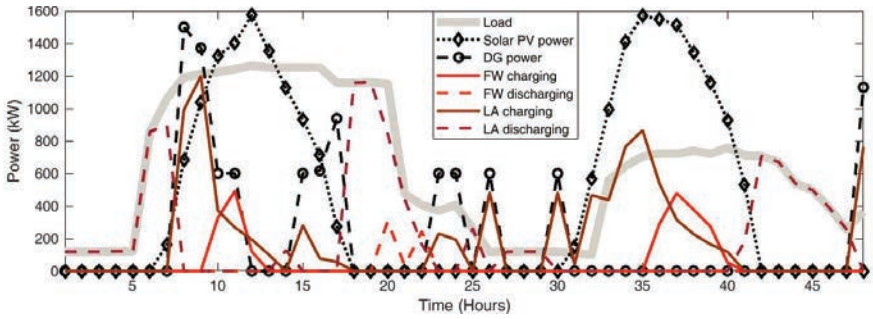

Figure 8 Power generation and consumption curve for Scenario-1, Case-1.

(a) *Case-1: Solar PV-DG- LA Battery-FW HPS*: In this case, solar PV is the primary source, with DG serving as a backup. Solar PV takes precedence over DG to feed the load. In case solar PV is unavailable, DG and ESS feed to load. The LA battery and the FW constitute the MESS. The power generated by each source, ESS, and power consumed by the load for a 48-hour duration is shown in Figure 8. It shows that when solar PV is available, it feeds the load. The DG also supports the load as a backup source. The LA battery stores the excess power generated by the solar PV for later uses. If the LA battery cannot charge, even if solar PV power is in excess, it is stored in the FW due to SoC constraints. The LA battery and FW support the load when solar PV is unavailable. In case the LA battery is prioritized over FW due to its less $\zeta_{\mathrm{O\&M}}$. Figure A-1 of the Appendix shows a similar variation for the whole year.

(b) *Case-2: Solar PV-DG-HSS-PEMFC-FW HPS*: The system is identical to that in Case-1, except the LA battery is replaced with another mid-term ESS, HSS with PEMFC. Figure 9 shows the plots for power generation during 48-hours. Here, the excess solar PV power feeds the electrolyzer cell to produce hydrogen stored in the hydrogen tanks, used by the PEMFC when load demands exceed the power generation. Once the hydrogen tank is full, then FW stores the excess power. Similarly, the excess load is met by the HSS first, then with FW during discharge. Figure A-2 of the Appendix shows a similar variation for the whole year.

(c) *Case-3: Solar PV-DG-LA HPS*: This case analyses the superiority of MESS over a single ESS. Here, the LA battery serves as the ESS, and the solar PV and DG are the primary sources. The solar PV and DG capacity are the same as Case-1 and Case-2. Figure 10 depicts the power generation

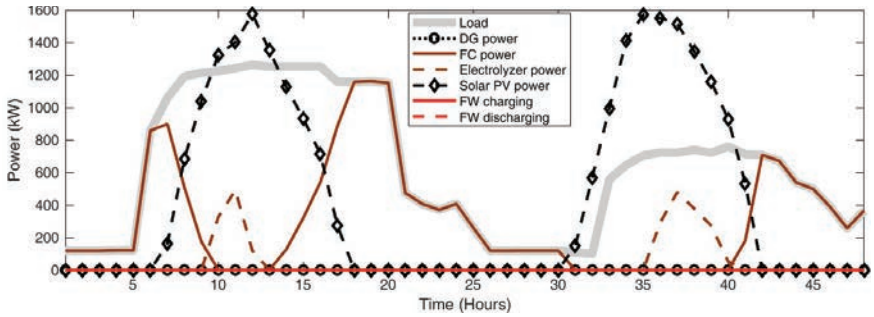

Figure 9 Power generation and consumption curve for Scenario-1, Case-2.

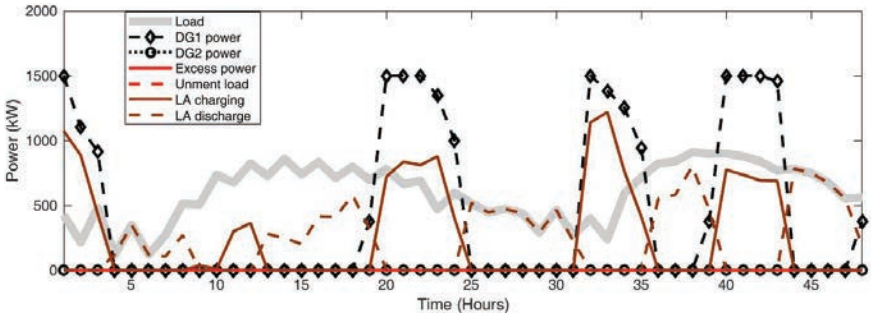

Figure 10 Power generation and consumption curve for Scenario-1, Case-3.

and consumption curve for over 48 hours. The use of MESS aids in energy wastage reduction while serving the load. Therefore, an extra DG is installed to support the load, increasing system cost and carbon emission. Figure A-3 of the Appendix shows a similar variation for the whole year.

(d) *Case-4: Solar PV-DG-FW HPS*: In this case, the LA battery of Case-3 is replaced with the short-term ESS, FW. The results are similar to those in Case-3. An extra DG is used to support the load. There are excess energy and unmet loads, as shown in Figure 11. Figure A-4 of the Appendix shows a similar variation for the whole year.

(e) *Case-5: Solar PV-DG-HSS-PEMFC HPS*: This case also considers a single ESS, HSS with PEMFC and electrolyzer. Here the excess solar PV power is wasted, as shown in Figure 12. The PEMFC and the DG support the load. An extra DG is not used since the PEMFC is unable to handle the extra loads. Figure A-5 of the Appendix shows a similar variation for the whole year.

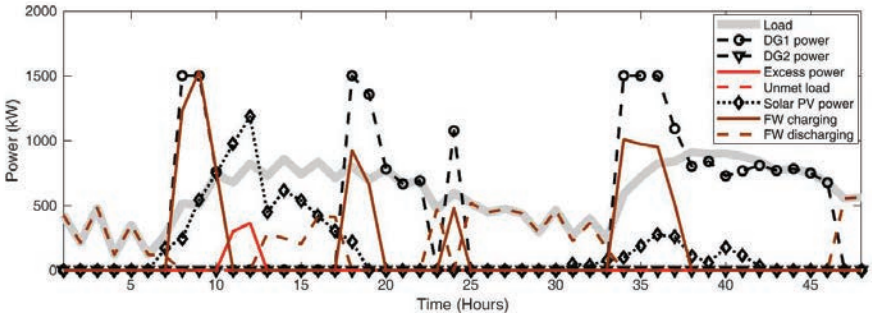

Figure 11 Power generation and consumption curve for Scenario-1, Case-4.

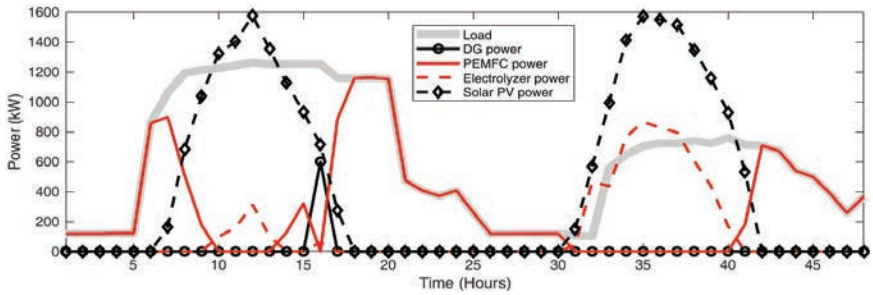

Figure 12 Power generation and consumption curve for Scenario-1, Case-5.

Table 3 NPC and LCOE analysis of Scenario-1

Cases	Net Present Cost (NPC) US $	Cost of Energy (LCOE) US $/kWh
Case-1	31760570	0.4525838
Case-2	17741730	0.25279
Case-3	33802600	0.481631
Case-4	36586900	0.521303
Case-5	21210070	0.302208

The NPC and LCOE for all five cases are tabulated in Table 3. It shows that Case-1 and Case-2 have the lowest NPC and LCOE. In Case-5, LCOE is less than in Case-3 and Case-4 due to the absence of extra DG. The LCOE of Case-5 is less than Case-1 due to the lack of FW and LA batteries. Though the LCOE of Case-5 is low, the case is infeasible as the load demand is not met due to the absence of MESS. Thus, Case-2 is the feasible solution with the lowest LCOE and zero energy wastage.

The pollutants, namely carbon dioxide, carbon monoxide, unburned hydrocarbons, particulate matter, Sulphur dioxide, and nitrogen oxide emitted

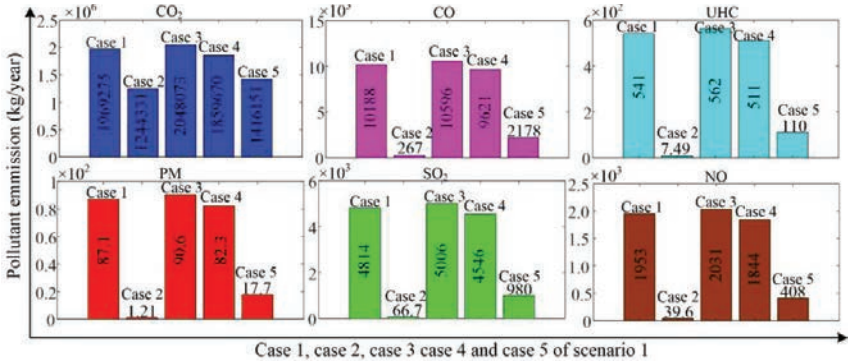

Figure 13 Pollutant emission in different cases of Scenario-1.

in each case, are shown in Figure 13. It indicates that Case-2 has relatively fewer pollutant emissions than other cases of Scenario-1.

4.2 Scenario-2

In this scenario, the FW and PH are employed as short-term and long-term ESS for the analysis. Depending on the combination, this scenario is analyzed in two cases as follows;

(a) Case-1: Solar PV-DG-FW-PH HPS.
(b) Case-2: Solar PV-DG-PH HPS.

(a) *Case-1: Solar PV-DG-FW-PH HPS*: In this case, solar PV is the primary energy source, and DG is the backup source. The combination of FW and PH forms the MESS. The power generation and consumption curve for the 48-hour duration is shown in Figure 14. The PH is prioritized over FW to support the load when the solar PV power is insufficient to meet the load. The excess solar PV power feeds the PH station until the capacity is reached; then, the FW is considered for storage. The FW discharges if the PH has insufficient capacity to meet the load during discharge. Figure A-6 of the Appendix shows a similar variation for the whole year.

(b) *Case-2: Solar PV-DG- PH HPS*: This case analyses the impact of using a single PH station as ESS. The PH feeds the load, while solar PV power is in deficit. An extra DG is used as a backup. The excess solar PV power charges the PH ESS. The power generation and consumption curve for 48-hours are shown in Figure 15. It shows that the surplus solar PV power generated is wasted after the total capacity of the PH station is utilized. Since FW is

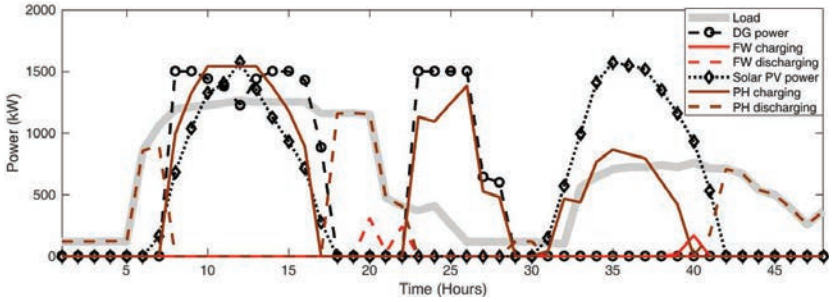

Figure 14 The power generation and consumption curve for Scenario-2, Case-1.

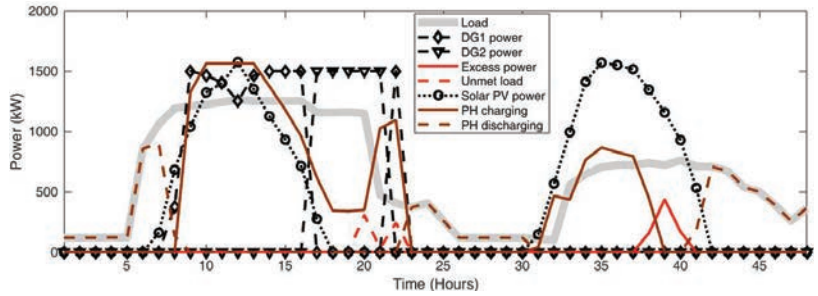

Figure 15 The power generation and consumption curve for Scenario-2, Case-2.

Table 4 NPC and LCOE analysis of Scenario-2

Cases	Net Present Cost (NPC) US $	Cost of Energy (LCOE) US $/kWh
Case-1	27386460	0.390212
Case-2	30950190	0.440989

analyzed in Scenario-1, Case-4, it is omitted in this scenario. Figure A-7 of the Appendix shows a similar variation for the whole year.

Table 4 tabulates the NPC and LCOE for the two cases. It shows that the LCOE of Case-1 is lower than Case-1. The pollutant emission is illustrated in Figure 16. Since the emissions are less in Case-1 than in Case-2, Case-1 is a feasible solution.

4.3 Scenario-3

This scenario considers the mid-term and long-term combinations of ESS to form the MESS. The LA battery and HSS with PEMFC and electrolyzer are

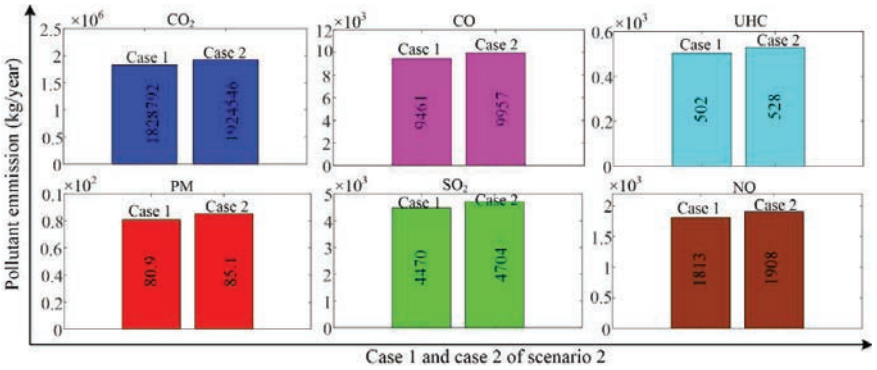

Figure 16 Pollutant emission in different cases of scenario 2.

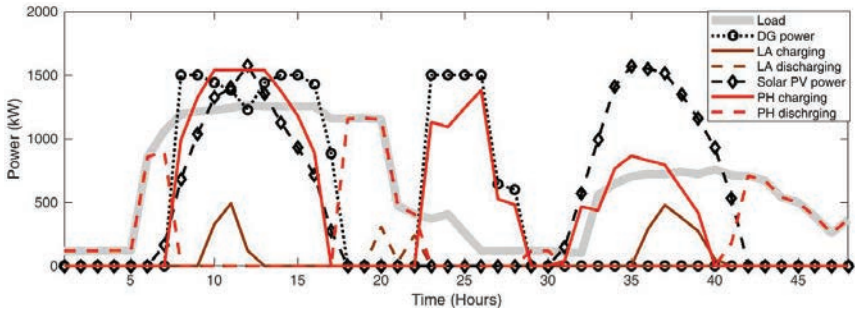

Figure 17 The power generation and consumption curve for Scenario-3, Case-1.

considered the mid-term ESS, and the PH station is considered a long-term ESS. The various cases below are analyzed in this scenario.

(a) Case-1: Solar PV-DG- LA Battery-PH HPS.
(b) Case-2: Solar PV-DG- HSS-PEMFC-PH HPS.

(a) *Case-1: Solar PV-DG- LA Battery-PH HPS*: In this case, the HPS consists of solar PV as the primary energy source, and DG serves as a backup. The LA battery and PH station are the ESS. The power generation and consumption curve for a 48-hour duration is shown in Figure 17. The PH station is given priority to support the load in the solar PV power deficit. The excess solar PV first charges the PH station, and then the LA battery is charged. During discharge, the PH station is also given priority over the LA battery. Figure A-8 of the Appendix shows a similar variation for the whole year.

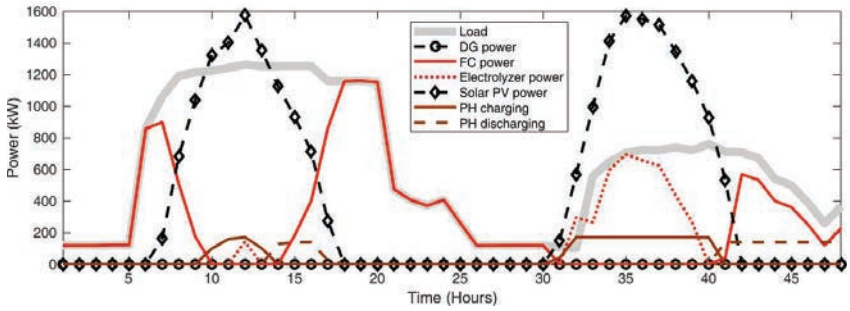

Figure 18 The power generation and consumption curve for Scenario-3, Case-2.

Table 5 NPC and LCOE analysis of Scenario-3

Cases	Net Present Cost (NPC) US $	Cost of Energy (LCOE) US $/kWh
Case-1	27386460	0.390212
Case-2	18203260	0.259366

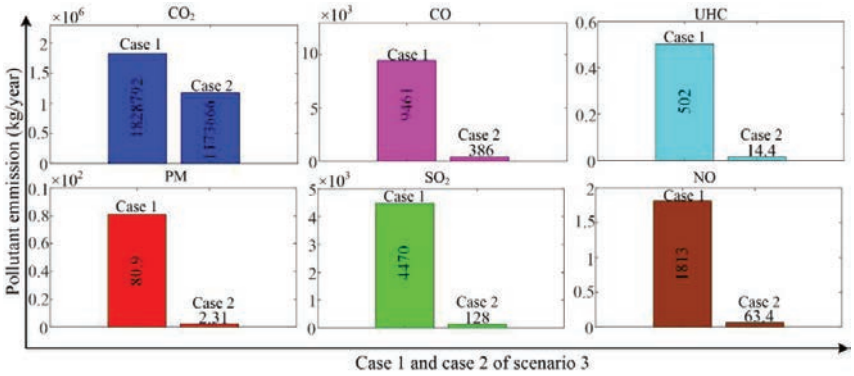

Figure 19 Pollutant emission in different cases of Scenario-3.

(b) *Case-2: Solar PV-DG- HSS-PEMFC-PH HPS*: The system is similar to Case-1 while replacing the LA battery with HSS-PEMFC and electrolyzer as ESS. The power generation and consumption curve for a 48-hours duration is shown in Figure 18. Here also, the PH station has prioritized charging and discharging over HSS-PEMFC. The excess solar PV power is diverted to the electrolyzer chamber after fully charging the PH station. Since the PEMFC supports the load as a backup source, the DG utilization is reduced. Figure A-9 of the Appendix shows a similar variation for the whole year.

For the scenario, the NPC and LCOE are tabulated in Table 5. Here, the LCOE of Case-2 is less than that of Case-1. The pollutant gas emission is

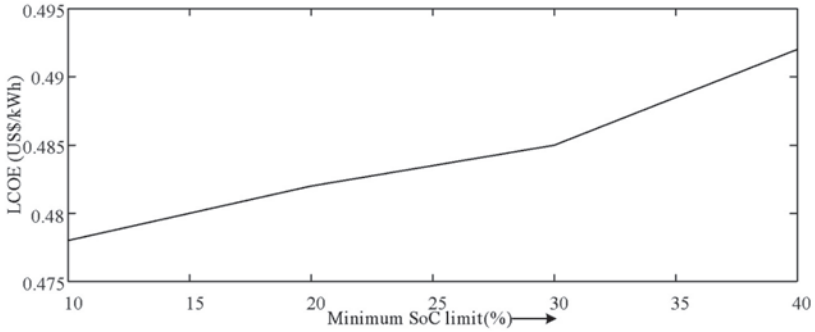

Figure 20 Variation of LCOE with minimum SoC limit.

plotted in Figure 19. The pollution is also less in Case-2. So, in this scenario, Case-2 is the feasible solution.

Summarily, three different scenarios are presented based on power generation of various sources, ESS charging and discharging curves, and pollutant emission. In Scenario-1, Case-2 is the feasible solution with the lowest LCOE and pollutant emission. For Scenario-2, Case-1 MES is the feasible solution. But in comparison to Scenario-1, this case is not feasible due to higher emission and LCOE. Amongst all the scenarios, Scenario-3, Case-2, i.e., the system with HSS with PEMFC and electrolyzer, is the most feasible solution with the lowest LCOE and pollutant emission.

4.4 Sensitivity Analysis

The sensitivity analysis is conducted to analyze the impact of the ESS SoC limit on the LCOE of the HPS. Case-1 from Scenario-1 is chosen here for the sensitivity analysis. The minimum SoC limit of the ESS is varied and plotted against the LCOE, as shown in Figure 20. It depicts that as the minimum SoC level decreases, the LCOE increases, which means that the lesser the DOD lesser is LCOE. Apart from the battery SoC limit, the interest rate and diesel price also affect the LCOE of the HPS.

5 Conclusion

Using the NPC and LCOE parameters, this paper examines the advantages of the MESS system over a single ESS. The analysis demonstrates that the MESS contributes to enhance the single ESS. It also aids in the reduction of pollutant emissions and energy waste by providing options for

electricity storage. The economics and temporal response features of ESS are additionally influenced by the subcategories of short-term, mid-term, and long-term ESS. The system with HSS, PEMFC, electrolyzer, and PH, Case-2 of Scenario-3, has the lowest LCOE and pollutant emission. This is owing to the system's lower average cost/kW. It can also be attributed to the ESS's comparable ratings in this scenario. Finally, a sensitivity analysis was conducted to investigate the impact of a change in the SoC limit on the LCOE. It observed that as the minimum SoC limit decreases, so does the LCOE.

Declaration of Interest Statement

The authors declare that they have no known competing financial interests or personal relationships that could have influenced the work reported in this paper.

Acknowledgments

The authors are very thankful to all the associated personnel in any reference that contributed to/for this research.

Funding

This research received no external funding.

Appendix

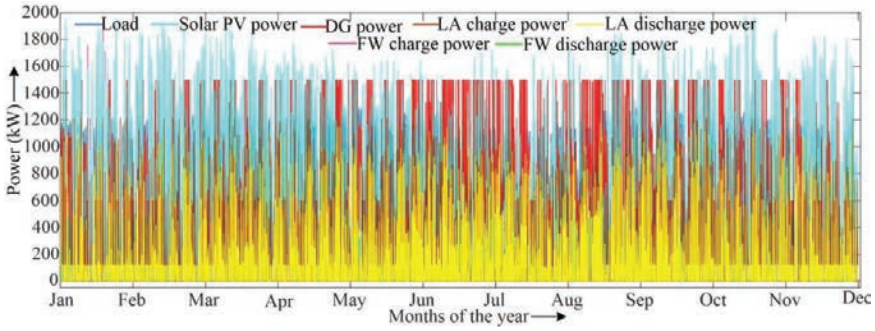

Figure A-1 Power generation-consumption curve for Scenario-1, Case-1.

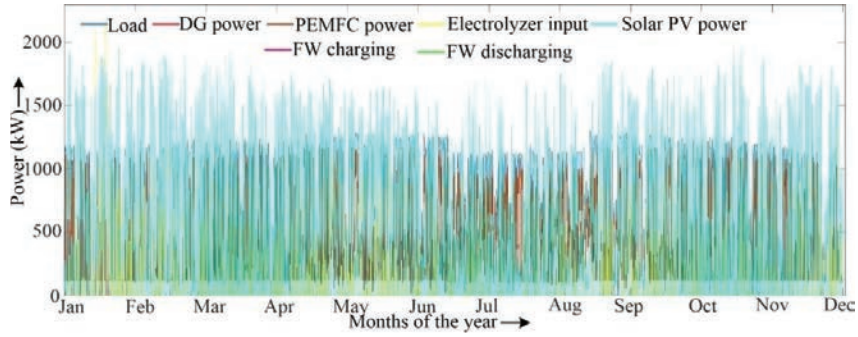

Figure A-2 Power generation-consumption curve for Scenario-1, Case-2.

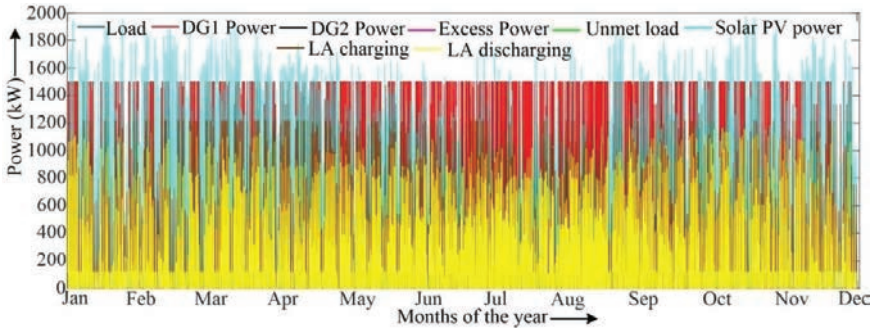

Figure A-3 Power generation-consumption curve for Scenario-1, Case-3.

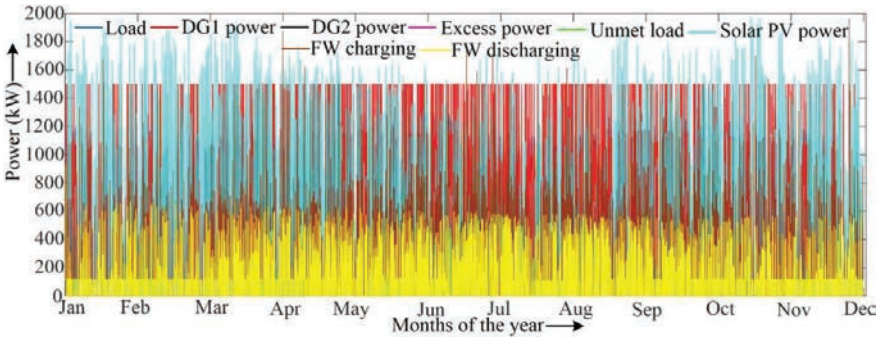

Figure A-4 Power generation-consumption curve for Scenario-1, Case-4.

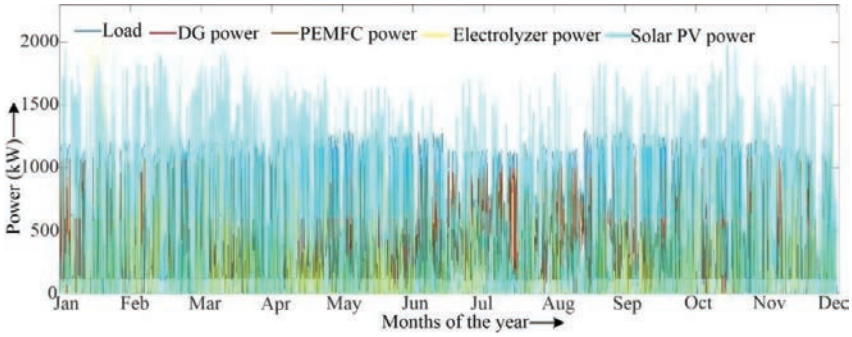

Figure A-5 Power generation-consumption curve for Scenario-1, Case-5.

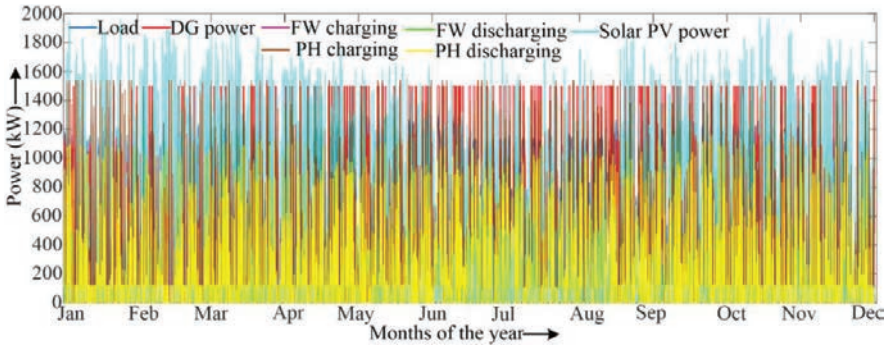

Figure A-6 Power generation-consumption curve for Scenario-2, Case-1.

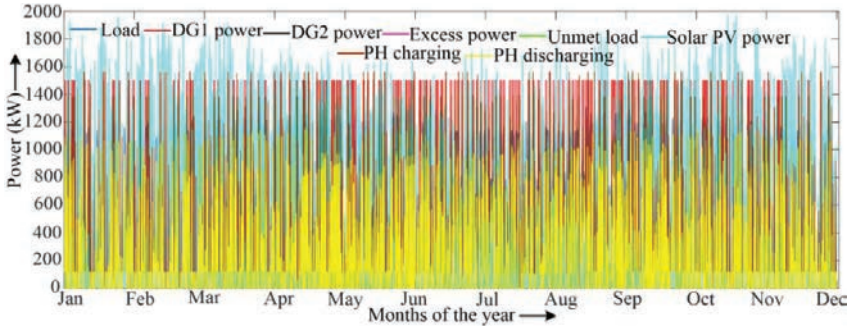

Figure A-7 Power generation-consumption curve for Scenario-2, Case-2.

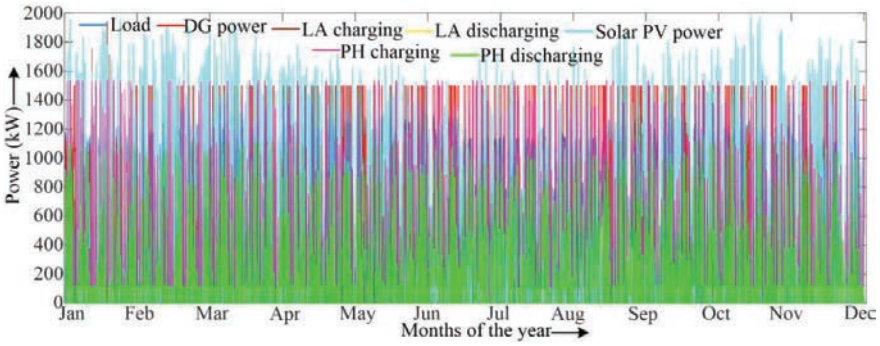

Figure A-8 Power generation-consumption curve for Scenario-2, Case-1.

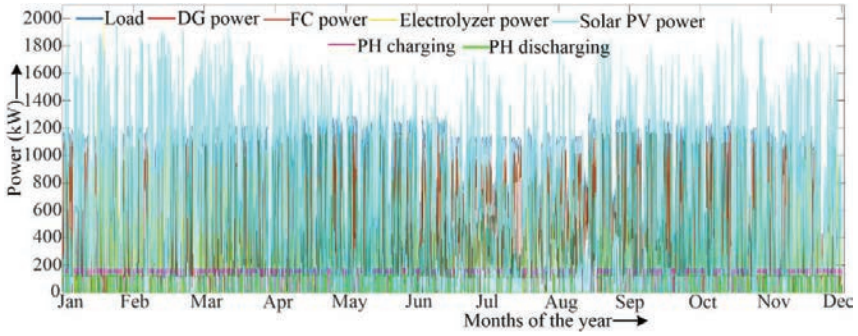

Figure A-9 Power generation-consumption curve for Scenario-3, Case-2.

References

[1] M.A. Jirdehi, V.S. Tabar, S. Ghassemzadeh, S. Tohidi, 'Different aspects of microgrid management: A comprehensive review,' J. Energy Storage, pp. 101–457, vol. 30, 2020. https://doi.org/10.1016/j.est.2020.101457.

[2] Huang, W. Liao, and H. Parvaneh, 'Optimal Scheduling of a Residential Energy Prosumer Incorporating Renewable Energy Sources and Energy Storage Systems in a Day-ahead Energy Market,' Distributed Generation & Alternative Energy Journal, pp. 265–294, vol. 35, no. 4, 2020. https://doi.org/10.13052/dgaej2156-3306.3542.

[3] M.H. Mostafa, S.H.E. Abdel Aleem, S.G. Ali, Z.M. Ali, A.Y. Abdelaziz, 'Techno-economic assessment of energy storage systems using annualized life cycle cost of storage (LCCOS) and levelized cost of energy (LCOE) metrics,' J. Energy Storage., vol. 29, 2020. https://doi.org/10.1016/j.est.2020.101345.

[4] P. Lata, S. Vadhera, 'Reliability Improvement of Radial Distribution System by Optimal Placement and Sizing of Energy Storage System using TLBO,' J. Energy Storage, pp. 101492, vol. 30, 2020. https://doi.org/10.1016/j.est.2020.101492.

[5] N. Eghtedarpour, E. Farjah, 'Power control and management in a Hybrid AC/DC microgrid,' IEEE Trans. Smart Grid., pp. 1494–1505, vol. 5, 2014. https://doi.org/10.1109/TSG.2013.2294275.

[6] J. Liu, C. Hu, A. Kimber, Z. Wang, 'Uses, Cost-Benefit Analysis, and Markets of Energy Storage Systems for Electric Grid Applications,' J. Energy Storage., pp. 101731, vol. 32, 2020. https://doi.org/10.1016/j.est.2020.101731.

[7] L.W. Chong, Y.W. Wong, R.K. Rajkumar, R.K. Rajkumar, D. Isa, 'Hybrid energy storage systems and control strategies for stand-alone renewable energy power systems,' Renew. Sustain. Energy Rev., pp. 174–189, vol. 66, 2016. https://doi.org/10.1016/j.rser.2016.07.059.

[8] M. Jami, Q. Shafiee, M. Gholami, H. Bevrani, 'Control of a supercapacitor energy storage system to mimic inertia and transient response improvement of a direct current micro-grid,' J. Energy Storage, pp. 101788, vol. 32, 2020. https://doi.org/10.1016/j.est.2020.101788.

[9] C.S. Karavas, K.G. Arvanitis, G. Kyriakarakos, D.D. Piromalis, G. Papadakis, 'A novel autonomous PV powered desalination system based on a DC microgrid concept incorporating short-term energy storage,' Sol. Energy., pp. 947–961, vol. 159, 2018. https://doi.org/10.1016/j.solener.2017.11.057.

[10] A. Omu, S. Hsieh, K. Orehounig, 'Mixed integer linear programming for the design of solar thermal energy systems with short-term storage,' Appl. Energy, pp. 313–326, vol. 180, 2016. https://doi.org/10.1016/j.apenergy.2016.07.055.

[11] J. Kondoh, T. Funamoto, T. Nakanishi, R. Arai, 'Energy characteristics of a fixed-speed flywheel energy storage system with direct grid-connection,' Energy, pp. 701–708, vol. 165, 2018. https://doi.org/10.1016/j.energy.2018.09.197.

[12] A. Kadri, H. Marzougui, A. Aouiti, F. Bacha, 'Energy management and control strategy for a DFIG wind turbine/fuel cell hybrid system with super capacitor storage system,' Energy, pp. 116518, vol. 192, 2020. https://doi.org/10.1016/j.energy.2019.116518.

[13] Karthikeyan, S., and R. Velraj. "Air heating with latent heat storage for thermal energy management of solar applications." Distributed Generation & Alternative Energy Journal, pp. 20–35, vol. 27, no. 4, 2012. https://doi.org/10.1080/21563306.2012.10554220.

[14] M.R. Sheibani, G.R. Yousefi, M.A. Latify, S.H. Dolatabadi, 'Energy storage system expansion planning in power systems: A review,' IET Renew. Power Gener., pp. 1203–1221, vol. 12, 2018. https://doi.org/10.1049/iet-rpg.2018.0089.

[15] M.A. Hannan, M. Faisal, P. Jern Ker, R.A. Begum, Z.Y. Dong, C. Zhang,, 'Review of optimal methods and algorithms for sizing energy storage systems to achieve decarbonization in microgrid applications,' Renew. Sustain. Energy Rev., pp. 110022, vol. 131, 2020. https://doi.org/10.1016/j.rser.2020.110022.

[16] I. Rahmati, A. Akbari Foroud, 'Pumped-storage units to address spinning reserve concerns in the grids with high wind penetration,' J. Energy Storage, pp. 101612, vol. 31, 2020. https://doi.org/10.1016/j.est.2020.101612.

[17] A. A. Kebede, T. Coosemans, M. Messagie, T Jemal, H. A. Behabtu, J. Van Mierlo, and M. Berecibar, M., 'Techno-economic analysis of lithium-ion and lead-acid batteries in stationary energy storage application,' Journal of Energy Storage, vol. 40, p. 102748. 2021. https://doi.org/10.1016/j.est.2021.102748.

[18] S. Ali, and C. M. Jang, 'Optimum design of hybrid renewable energy system for sustainable energy supply to a remote island,' Sustainability, p. 1280, vol. 12, no. 3, 2020. https://doi.org/10.3390/su12031280.

[19] S. Dhundhara, Y.P. Verma, A. Williams, 'Techno-economic analysis of the lithium-ion and lead-acid battery in microgrid systems, Energy Convers. Manag,' pp. 122–142, vol. 177, 2018. https://doi.org/10.1016/j.enconman.2018.09.030.

[20] I. Pawel, 'The cost of storage - how to calculate the levelized cost of stored energy (LCOE) and applications to renewable energy generation,' pp. 68–77, vol. 46, 2014. https://doi.org/10.1016/j.egypro.2014.01.159.

[21] V. M. M. Suresh, R. Kiranmayi, 'Modelling and optimization of an off-grid hybrid renewable energy system for electrification in a rural areas,' Energy Reports, pp. 594–604, vol. 6, 2020. https://doi.org/10.1016/j.egyr.2020.01.013.

[22] V. Boddapati, S. A. Daniel, 'Design and Feasibility Analysis of Hybrid Energy-Based Electric Vehicle Charging Station,' Distributed Generation & Alternative Energy Journal, pp. 41–72, vol. 37, no. 1, 2022. https://doi.org/10.13052/dgaej2156-3306.3713.